Optimum Battery Size for Fuel Cell Hybrid Electric Vehicle With Transient Loading Consideration—Part II

Olle Sundström[1]
Measurement and Control Laboratory,
Swiss Federal Institute of Technology,
CH-8092 Zurich, Switzerland
e-mail: olles@ethz.ch

Anna Stefanopoulou
Department of Mechanical Engineering,
University of Michigan,
Ann Arbor, MI 48109
e-mail: annastef@umich.edu

This study presents a simplified model of a midsized vehicle powered by a polymer electrolyte membrane fuel cell stack together with a lead-acid battery as an energy buffer. The model is used with dynamic programming in order to find the optimal coordination of the two power sources while penalizing transient excursions in oxygen concentration in the fuel cell and the state of charge in the battery. The effects of the battery size on the overall energy losses for different drive cycles are determined, and the optimal power split policies are analyzed to quantify all the energy losses and their paths in an effort to clarify the hybridization needs for a fuel cell vehicle with constraints on dynamically varying variables. Finally, a causal nonpredictive controller is presented. The battery sizing results from the dynamic programming optimizations and the causal controller are compared. [DOI: 10.1115/1.2713779]

Keywords: fuel cell vehicle, dynamic programming, hybridization

1 Introduction

Fuel cell systems (FCS) can be used as a primary power source for both automotive applications and stationary power applications. Using an energy buffer together with the FCS can provide benefits such as reduced hydrogen consumption and assistance during transient loading. The hybridization levels for reduced hydrogen consumption of an automotive system are addressed in [1], where it is shown that when not considering regenerative braking, hybridization of automotive fuel cell systems will not always improve fuel economy. The hybridization levels for protecting the FCS from abrupt load variations that can cause reactant starvation are clarified here. Long reactant starvation periods can lead to decreased performance and permanent damage of the fuel cell membrane. Judicious hybridization can thus extend the lifetime of FCS, which is currently one of the technical hurdles associated with FCS.

Hybridization can provide assistance during FCS transient loading and thus reduce oxygen starvation in both automotive and stationary fuel cell applications. In general, the hydrogen at the anode is provided by a pressurized hydrogen storage and the oxygen at the cathode is provided by a compressor. We will only consider oxygen starvation in this study and assume an instantaneous hydrogen supply.

To prevent oxygen starvation, an excess oxygen supply is desired. However, an increase in oxygen supply increases the parasitic losses associated with increased compressor output. In this paper, the effects of different lead-acid battery sizes in a fuel cell hybrid electric vehicle have been analyzed when the FCS oxygen excess ratio (OER) needs to meet certain constraints. Note that particle matter and smoke in Diesel engine exhaust forms during transient loading, and thus our approach, could be applied to an ICE Diesel-hybrid vehicle. In this paper, the power split is first achieved through dynamic programming (DP) [2] optimization. The DP results represent the best-possible sequence of commands, which can only be achieved by knowing a priori the course that will be driven. The power split derived through DP is a-causal. As it is shown later, the optimum power split policy often dictates an increase in FCS power before an increase in the requested power. This precompensation helps reduce excursions in OER and battery state of charge (SOC), but cannot be realized when the future power demand is not known, as in a typical driving scenario.

In the last part of this paper, the power split is controlled by a simple nonlinear and causal controller. The results associated with the FCS performance and the battery sizing for the two control schemes are compared and analyzed.

When hybridizing a power train, it is challenging to size the battery because the drive cycle [3,4], the control policy [5], and the hardware architecture [6] affect the optimal size. When increasing the battery size in a hybrid electric vehicles, the total vehicle weight increases, which affects the fuel consumption. In stationary fuel cell applications, the weight is not as important as in automotive applications; thus, if the same approach is used to size an energy buffer, additional performance variables, such as cost or volume, have to be included in the DP optimization.

When making the decision to include a battery or another energy buffer in the power train, it is important to consider the actual costs of the battery and the added complexity associated with hybridization [3,7]. The prices on fuel cells and batteries vary with time; we will therefore only focus on determining the effects of hybridization on hydrogen consumption and stack oxygen excess ratio. We do not know how detrimental to the FCS life are periods of low excess oxygen ratio; thus, we choose an arbitrary function to penalize deviations of OER.

Section 2 describes the fuel cell hybrid electric vehicle (FCHEV) model. Section 3 shows the dynamic programming method and results. In Sec. 4, a simple causal controller is presented and a comparison to the dynamic programming results is presented. Finally, in Sec. 5, a discussion and some conclusions from the results are discussed as well as possible future work.

[1]This work was done at the Fuel Cell Control System Laboratory at the University of Michigan, Ann Arbor. Olle Sundström is now affiliated with the Measurement and Control Laboratory at the Swiss Federal Institute of Technology, Zurich.

Submitted to ASME for publication in the JOURNAL OF FUEL CELL SCIENCE AND TECHNOLOGY. Manuscript received May 3, 2006; final manuscript received December 20, 2006. Review conducted by Ken Reifsnider. Paper presented at the IEEE International Conference on Control Application, October 4–6 2006, Munich Germany.

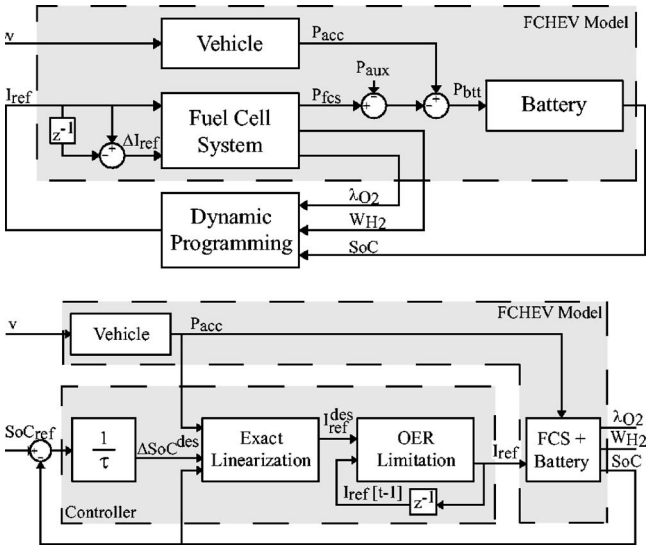

Fig. 1 Signal flow overview of the two methods used to control the power split in the FCHEV. Top figure (*a*) shows the signal flow during the dynamic programming optimizations. Bottom figure (*b*) shows an overview of the proposed controller and the signal flows between the controller and the FCHEV model.

2 Method

To investigate how battery size affects the optimum FCS buffering during transient loading, we will first use deterministic DP and then a simple causal and nonpredictive controller. The DP methodology weights hydrogen consumption, excursions from the nominal fuel cell oxygen concentration and excursions from the nominal battery state of charge as shown in Fig. 1(*a*). The simple causal nonpredictive controller is used to control the battery state of charge as shown in Fig. 1(*b*). Details of each methodology are discussed in Secs. 3.1 and 4.1, respectively. The energy losses associated with each strategy and with various battery sizes are analyzed. The optimum battery sizes for the optimal power split policies are also compared to the optimum results when the fuel cell oxygen concentration is not penalized. This section describes the FCHEV model and the drive cycles used to evaluate the component sizes.

2.1 FCHEV Model. The FCHEV model, similar to [1], is separated into three components: fuel cell system, vehicle, and battery pack. Figure 1(*a*) shows the three components and how they interact with each other during the DP optimizations, and Fig. 1(*b*) shows how the three components interact when using the proposed controller. The FCHEV model is a simplified version of the detailed model in [8]. When using DP to solve optimal control problems, it is crucial to minimize the number of states and the computation time of the model due to the computational complexity of the DP algorithm. This is done by approximating fast dynamics as instantaneous and employing nonlinear static maps to model their associated steady state behavior. Forward Euler approximation, with a sampling interval of 1 s, is used to discretize the continuous in time state equations before using DP and the proposed controller. The parameters in the model are shown in Table 1.

2.1.1 Fuel Cell System. The FCS is the primary energy source in the vehicle that supplies electric energy to the voltage bus in the vehicle. An important FCS performance variable is the oxygen excess ratio (OER), which is the mass airflow rate supplied to the cathode divided with the mass airflow rate needed for the oxygen reaction associated with the current drawn from the fuel cell. Maintaining high OER helps in reducing the possibility of oxygen starvation in the fuel cell stack. Steady-state regulation of OER is shown to be achieved by a feedforward compressor controller [9]. During fast changes in current drawn, it is not possible to maintain the desired OER value due to the manifold filling and compressor inertial dynamics. It is hence important to develop an optimal power-splitting policy based on its effects on OER excursions. To penalize OER excursions in the DP cost function, we extend the model presented in [1] by introducing an extra state that allows through the map in Fig. 2 to access the worst OER, λ_{O_2}, during changes in reference current I_{ref}: $\lambda_{O_2}=g(I_{\text{ref}},\Delta I_{\text{ref}})$, where $\Delta I_{\text{ref}}(k)=I_{\text{ref}}(k)-I_{\text{ref}}(k-1)$. The map g is calculated using the original FCS model [8], which includes (i) a feedforward compressor map that maintains a steady-state OER at 2, and (ii) the dynamics of compressor and manifolds. With the map g and the additional state, we manage to accurately capture OER excursions without the three extra states of the FCS model in [8].

Two examples of the worst OER value during step changes in the reference current are shown in Fig. 3. A step increase of 10 A from 110 A to 120 A causes OER to drop to 1.77. The worst OER value of 1.77 is thus data point (a) in Fig. 2. A step of 10 A from 10 A to 20 A causes OER to drop momentarily down to 1.0 as shown in Fig. 3 and summarized with data point (b) in Fig. 2.

The rest of the FCS model is the same as the one in [1]. The total energy in the used fuel during the cycle E_{H_2} is

$$E_{\text{H}_2}=Q_{\text{HHV}}^{\text{H}_2}\int_0^T W_{\text{H}_2}dt\ [\text{J}] \tag{1}$$

The hydrogen consumption W_{H_2} is a function of the current drawn from the FC stack, I_{st}, which, in turn, is a function of the net

Table 1 Model parameters

Mass (without battery) (m_0)	1384 kg
Rolling resistance coefficient (K_f)	0.02
Aerodynamic drag coefficient (C_d)	0.312
Frontal area (A)	2.06 m^2
Cells (n_{cell})	381
Maximum net power ($P_{\text{fcs}}^{\max}$)	54 kW
Auxiliary power (fixed) (P_{aux})	500 W
OER limit ($\lambda_{O_2}^{\lim}$)	1.75
Faraday's constant (F)	9.6485×10^4
Hydrogen molarmass (M_{H_2})	2.016×10^{-3} kg/mol
Hydrogen energy content ($Q_{\text{HHV}}^{\text{H}_2}$)	141.9×10^6 J/kg
Gasoline energy content ($Q_{\text{HHV}}^{\text{gas}}$)	46.7×10^6 J/kg
Gasoline density (ρ_{gas})	733.22 kg/m^3
Mass (m_{btt})	6.68 kg
Capacity (q_{btt})	18 Ah
Maximum output power (SoC=0.6)	2.78 kW
Charging efficiency (η_{btt}, $I_{\text{btt}}<0$)	0.9
SoC reference (SoC_{ref})	0.6

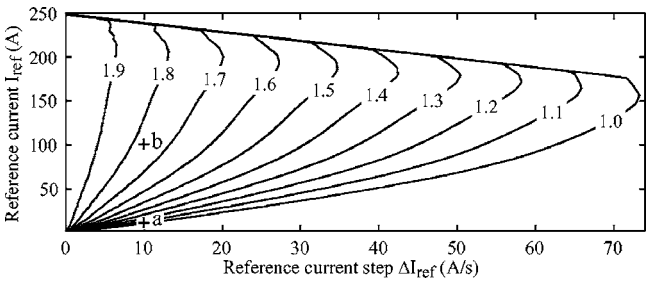

Fig. 2 Oxygen excess ratio map used to calculate the OER in the fuel cell system when changing the reference current. The examples (*a*) and (*b*) shown in Fig. 3 are also marked.

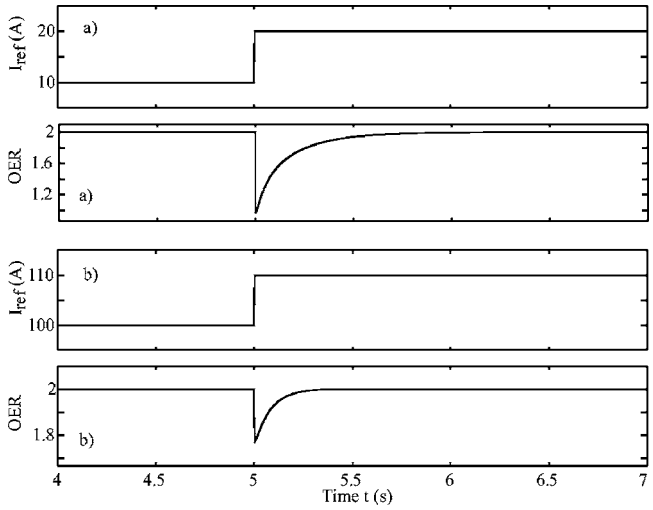

Fig. 3 Steps in the reference current and the resulting oxygen excess ratio. A step of 10 A from 10 A (*a*) and the resulting OER drop, and a step of 10 A from 100 A (*b*) and the resulting OER drop.

current out of the FCS I_{ref} dictated by the controller.

The total energy out from the FCS E_{fcs} is

$$E_{fcs} = \int_0^T (P_{fcs} - P_{aux})dt \text{ [J]} \tag{2}$$

where P_{aux} is a fixed power demand from all the other FCS auxiliary devices and P_{fcs} is the FCS output power, which is a function of the net FCS current as in [1]. The maximum FCS power is $P_{fcs}^{max} \approx 54$ kW and occurs at $I_{ref}=248$ A. Further increase in the current drawn from the FCS decreases the net FCS power so the FCS reference current is limited to $I_{ref} \leq I_{ref}^{max}=248$ A throughout this study.

The FCS efficiency is

$$\eta_{fcs} = \frac{P_{fcs} - P_{aux}}{Q_{HHV}^{H_2} W_{H_2}} \tag{3}$$

where $Q_{HHV}^{H_2}$ is the energy content of hydrogen (using higher heating value). The cycle average FCS efficiency is

$$\bar{\eta}_{fcs} = \frac{E_{fcs}}{E_{H_2}} \tag{4}$$

The parameters in the FCS model are shown in Table 1.

2.1.2 Vehicle. The vehicle mass 1384 kg includes the FCS and hydrogen storage and excludes the mass of the battery pack. The power demand P_{dem} is

$$P_{dem}(m,t) = v(t)\left[m\dot{v}(t) + K_f mg + \frac{\rho_{air} C_d A}{2} v^2(t)\right] \text{ [W]} \tag{5}$$

The acceleration power demand, $P_{acc}(t)$ is the positive part of the power demand, P_{dem} (5), is provided by the fuel cell system and the battery pack. The deceleration power demand is assumed to be absorbed by nonregenerative braking.

2.1.3 Battery Pack. The battery pack model is the same with the one used in [1] and is based on an ADVISOR model [10]. The battery output/input power P_{btt} is the remaining power to meet the drive-cycle power demand

$$P_{btt}(t) = P_{acc}(t) - (P_{fcs}(t) - P_{aux}) \text{ [W]} \tag{6}$$

where P_{acc} is the acceleration power demand and $(P_{fcs}-P_{aux})$ is the FCS net output power. The battery current I_{btt} is a function of the battery's state of charge, as in [1]. The battery's state of charge (SoC) is calculated using

$$\frac{d}{dt}[\text{SoC}(t)] = \frac{-I_{btt}(t)\,\eta_{btt}[I_{btt}(t)]}{3600 q_{btt}} \tag{7}$$

where η_{btt} is the battery charging efficiency [1]. The input power, i.e., charging current, to the battery has not been limited, and all the charging power from the FCS and the regenerative braking is assumed to be absorbed by the battery.

Table 2 Drive-cycle characteristics and the power characteristics when $n_{btt}=10$ and $m=1451$ kg

Cycle	NYCC	FTP-72	SFTP
Average power			
Acc. (kW)	4.9	7.2	21.5
Brk. (kW)	4.1	7.0	17.3
Max power			
Acc. (kW)	25.7	31.8	80.1
Brk. (kW)	21.6	23.4	53.8
Top speed (km/h)	44.6	91.3	129.2
Duration (s)	599	1370	601
Distance (m)	1898	11990	12888
$E_{acc}^{m_0}$ (14) (MJ)	1.024	5.748	8.980

2.2 Drive Cycles. The power demand from the drive cycles is calculated backward using the discretized version of the vehicle model (5). The three drive cycles are New York City Cycle (NYCC), which represents low speed and mild driving; federal test procedure—72 cycle (FTP-72), which represents both low-speed city driving and moderate highway driving; and supplemental federal test procedure cycle (SFTP), which represents aggressive high-speed driving. The drive cycles, and their power characteristics for a vehicle with ten battery modules and a mass of 1451 kg, are summarized in Table 2.

3 Dynamic Programming Optimizations

This section shows the DP method and the results from the DP optimizations. The general signal flow during the optimizations is shown in Fig. 1(*a*), where v is the speed given by the drive cycles and I_{ref} is the input reference current to the FCS. The three performance variables, the battery's state of charge SoC, the hydrogen consumption in the FCS W_{H_2}, and the OER in the FCS λ_{O_2} are used to calculate the cost function for the DP optimization. We will investigate, as in [1], the energy losses in the different components and how they change with the battery size.

3.1 Dynamic Programming Method. The main DP equations, equivalent to [1], are shown in Appendix. To incorporate the OER dynamics in the optimization, however, an additional state is introduced compared to [1]. Moreover, the cost function, J, has to be redefined as

$$J = (\alpha \Delta \text{SoC})^2 + \beta W_{H_2} + (\gamma \Delta \lambda_{O_2})^2 \tag{8}$$

$$\Delta \text{SoC} = \text{SoC} - \text{SoC}_{ref} \tag{9}$$

$$\Delta \lambda_{O_2} = \begin{cases} \lambda_{O_2}^{lim} - \lambda_{O_2}, & \lambda_{O_2} < \lambda_{O_2}^{lim} \\ 0, & \lambda_{O_2} \geq \lambda_{O_2}^{lim} \end{cases} \tag{10}$$

where ΔSoC is the deviation of the battery's state of charge from the reference value SoC_{ref}, W_{H_2} is the hydrogen consumption in the FCS, $\Delta\lambda_{O_2}$ is the deviation of the minimum OER (when changing the reference current) below a limiting value $\lambda_{O_2}^{lim}$, and $\{\alpha, \beta, \gamma\}$ are weights. FCS or battery deterioration are not in-

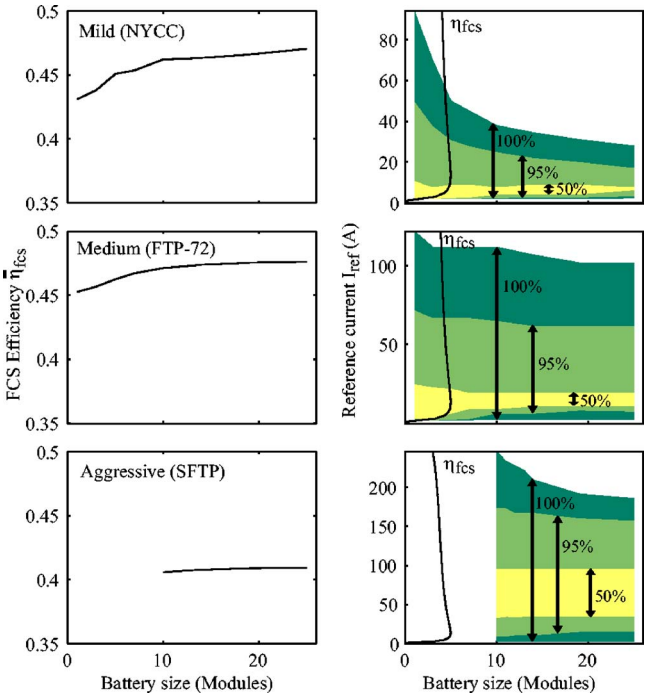

Fig. 4 Fuel cell system efficiency, $\bar{\eta}_{FCS}$, (left) together with the reference current distribution (right) for different battery sizes and drive cycles (using DP). The FCS efficiency curve is shown in the left part of the reference current distribution plot.

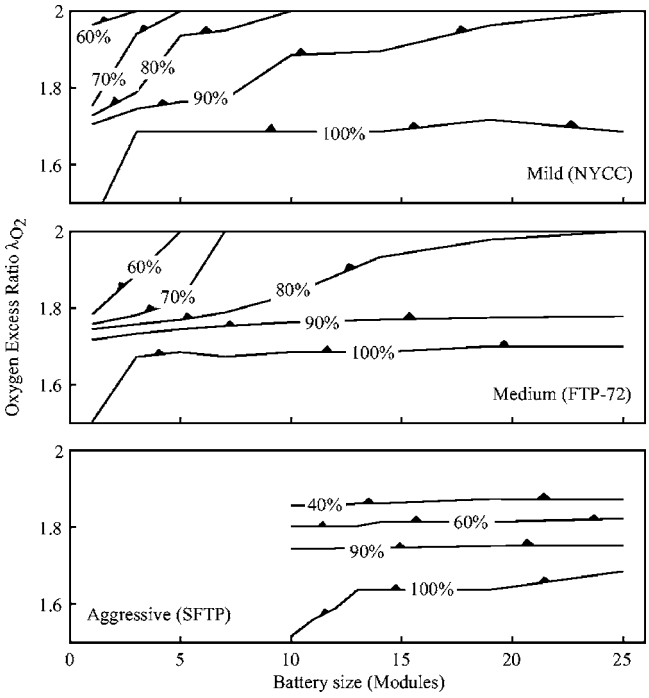

Fig. 5 The OER distributions for different battery sizes for the three drive cycles. The percentages gives how much of the time is spent above the OER values.

cluded in the model (which are associated with FCS oxygen starvation and repetitive large battery charging and discharging). Therefore, large OER deviations (during reference current increments) and large battery state-of-charge deviations are heavily penalized to include deterioration, hence the quadratic cost functions. The weights α, β, and γ in (8) are set so that when $\Delta\text{SoC}=0.1$, $W_{H_2}=W_{H_2}(I_{ref}^{max})=0.0013$ kg/s, and $\lambda_{O_2}=1.5$ then $(\alpha\Delta\text{SoC})^2=\beta W_{H_2}=(\gamma\Delta\lambda_{O_2})^2=J/3=1$, i.e., each performance variable contributes equally to the cost. An OER limit, $\lambda_{O_2}^{lim}=1.75$ has been used throughout this study. The SoC operating point is set to the optimal value $\text{SoC}_{ref}=0.6$ from the analysis in [1] throughout this study.

3.2 Dynamic Programming Results. This section shows how DP adjusts the FCS reference current and the implications of the DP decisions on the FCS efficiency, the energy loss in the battery, and the energy loss due to the added weight with increasing battery size for the different drive cycles.

3.2.1 Fuel Cell System. The average FCS efficiency (4) is shown in the left column of Fig. 4. When increasing the battery size the FCS efficiency increases. This increase is caused, as in [1], by decoupling the acceleration power demand, P_{acc}, from the FCS output power, P_{fcs}. The right column of Fig. 4 shows the distribution of the FCS reference current I_{ref} for different sizes together with the FCS efficiency curve η_{fcs} (3). The changes of these distributions are similar to those in [1]. When increasing the battery size, the DP shifts the inefficient current levels toward higher efficiencies. The average FCS efficiencies achieved now are larger than the ones observed when OER was not penalized [1] because the peak reference current and very low reference current levels that typically cause large OER excursions are now rare. The peak reference current now shift to lower values with high FCS efficiency as shown in Fig. 4 (right column).

The resulting OER distributions for the different drive cycles and battery sizes are shown in Fig. 5. For example, with a battery size of five modules in the medium cycle (FTP-72) the OER is higher than 1.8, 70% of the time, and higher than 1.68, 100% of the time. Furthermore, with a battery size of 19 modules in the mild cycle (NYCC) the OER is higher than 1.7, 100% of the time and higher than 1.95, 90% of the time.

3.2.2 Battery. The electrical energy expended in the battery is

$$E_{loss}^{btt}=\left|\int_0^T P_{btt}dt\right| \text{ [J]} \tag{11}$$

where P_{btt} is the battery power.[2] The hydrogen energy required to produce the electric energy expended in the battery is $E_{loss}^{btt}/\bar{\eta}_{fcs}$, where $\bar{\eta}_{fcs}$ is the cycle average FCS efficiency. The energy expended in the battery, E_{loss}^{btt}, together with the hydrogen equivalent energy, $E_{loss}^{btt}/\bar{\eta}_{fcs}$, are shown in the left column of Fig. 6.

For the mild and medium cycles the expended battery energy decreases rapidly at first but then levels out for larger battery sizes. For the aggressive cycle, the expended battery energy is also decreasing with increasing battery size. This is because the DP is forced, through the added cost in (8), to use the battery to maintain the OER at a high levels. This is hard for small batteries and will therefore result in larger expended energy in the battery.

3.2.3 Added Mass. The energy loss due to the added mass, when increasing the battery size, affects the performance of the vehicle. We define the energy loss due to the added mass as

$$E_{loss}^{\Delta m}=E_{acc}^{m}-E_{acc}^{m_0} \text{ [J]} \tag{12}$$

where the total acceleration energy for a vehicle with n_{btt} battery modules is

[2]Note that even though the DP ensures that $\text{SoC}(T)\approx\text{SoC}(0)$ there is always energy expended in the battery ($E_{loss}^{btt}>0$) due to losses in the internal resistance and due to the charging efficiency, η_{btt} [1].

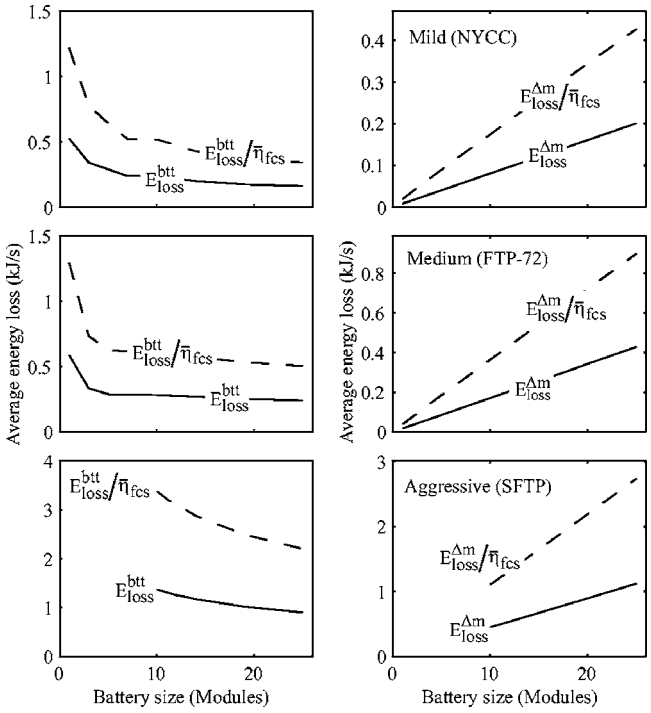

Fig. 6 Average electric energy expended in the battery and its equivalent hydrogen energy (left) together with the average electric energy loss due to the added mass and its equivalent hydrogen energy loss (right) (using DP)

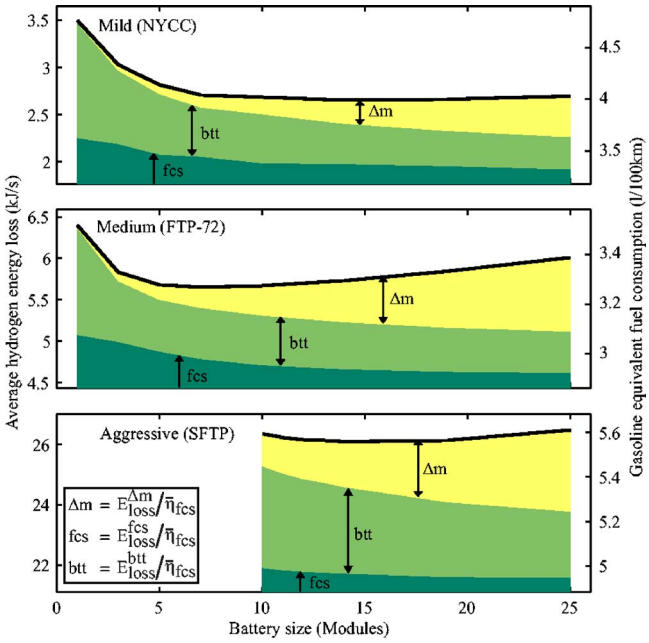

Fig. 7 The average energy loss per second in the three drive cycles (using DP). Equivalent hydrogen energy loss from added weight (Δm), expended energy in the battery (btt), and FCS energy loss (fcs). The solid line shows the gasoline equivalent fuel consumption C^V_{gas}.

$$E^m_{\text{acc}} = \int_0^T P_{\text{acc}}(m_0 + n_{\text{btt}} m_{\text{btt}}, t)dt \ [\text{J}] \tag{13}$$

and the total acceleration energy for a vehicle without battery pack is

$$E^{m_0}_{\text{acc}} = \int_0^T P_{\text{acc}}(m_0, t)dt \ [\text{J}] \tag{14}$$

The parameters m_0 and m_{btt} are shown in Table 1. The energy loss due to the added mass $E^{\Delta m}_{\text{loss}}$ and the hydrogen equivalent energy loss $E^{\Delta m}_{\text{loss}}/\bar{\eta}_{\text{fcs}}$ are shown in the right column of Fig. 6. The energy loss $E^{\Delta m}_{\text{loss}}$ is increasing proportional to the battery size for all three drive cycles. Note that an increase in battery size corresponds to an increase in vehicle weight and net vehicle power because the FCS power size remains fixed.

3.2.4 System. The total hydrogen energy lost during a cycle is defined as the hydrogen energy used during the cycle minus the energy supplied to meet the acceleration power demand for the original vehicle mass, m_0

$$E^0_{\text{loss}} = E_{\text{H}_2} - E^{m_0}_{\text{acc}} \ [\text{J}] \tag{15}$$

The total hydrogen energy lost, E^0_{loss}, is separated into

$$E^0_{\text{loss}} = \frac{E^{\text{fcs}}_{\text{loss}}}{\bar{\eta}_{\text{fcs}}} + \frac{E^{\text{btt}}_{\text{loss}}}{\bar{\eta}_{\text{fcs}}} + \frac{E^{\Delta m}_{\text{loss}}}{\bar{\eta}_{\text{fcs}}} \tag{16}$$

where $E^{\text{btt}}_{\text{loss}}/\bar{\eta}_{\text{fcs}}$ is the hydrogen equivalent energy expended in the battery, $E^{\Delta m}_{\text{loss}}/\bar{\eta}_{\text{fcs}}$ is the hydrogen equivalent energy loss due to the added mass, and $E^{\text{fcs}}_{\text{loss}}/\bar{\eta}_{\text{fcs}}$ is the remaining hydrogen equivalent energy loss in the FCS. The electric energy expended in the battery, $E^{\text{btt}}_{\text{loss}}$, is defined in (11), and the electric energy loss due to added weight is defined in (12).

Taking into account the electric energy expended in the battery, $E^{\text{btt}}_{\text{loss}}$, defined in (11) and the electric energy loss due to added weight defined in (12), the remaining electric energy loss in the FCS is then calculated using

$$E^{\text{fcs}}_{\text{loss}} = \bar{\eta}_{\text{fcs}} E^0_{\text{loss}} - E^{\text{btt}}_{\text{loss}} - E^{\Delta m}_{\text{loss}} \ [\text{J}] \tag{17}$$

similarly to [1].

The total hydrogen energy loss, E^0_{loss}, is proportional to the gasoline equivalent fuel consumption[3]

$$C^V_{\text{gas}} = 10^8 \frac{E^0_{\text{loss}} + E^{m_0}_{\text{acc}}}{Q^{\text{gas}}_{\text{HHV}} \rho_{\text{gas}} \int_0^T v dt} \left[\frac{1}{100 \text{ km}}\right] \tag{18}$$

where $Q^{\text{gas}}_{\text{HHV}}$ is the energy content of gasoline (based on the higher heating value) and ρ_{gas} is the gasoline density.

The total hydrogen energy loss, the hydrogen equivalent energy loss due to the added weight, and the hydrogen equivalent energy expended in the battery are shown in Fig. 7. For the mild cycle, the large energy expended in the battery for small battery sizes makes it inefficient to have less battery modules than 10–20. For the medium cycle, the large energy expended in the battery for small battery sizes together with the large energy loss due to the added weight for large batteries introduce an optimal battery size of five to ten modules. In the aggressive cycle, the decrease in expended battery energy is almost equivalent to the energy loss due to added weight. However, there is an optimal battery size of 15 modules.

4 Comparison to Fixed Structure Controller

Since DP is predictive and noncausal, this section introduces a very simple controller to control the state of charge in the battery pack. The resulting controller is used to compare the battery sizing using the predictive optimal DP method to a nonpredictive con-

[3]Note that the gasoline equivalent fuel consumption is measured in $l/100$ km and that the US fuel economy, measured in miles per gallon, is $C^V_{\text{gas}}|_{\text{US}} \approx 235.2 \cdot (C^V_{\text{gas}})^{-1}$ *mpg*.

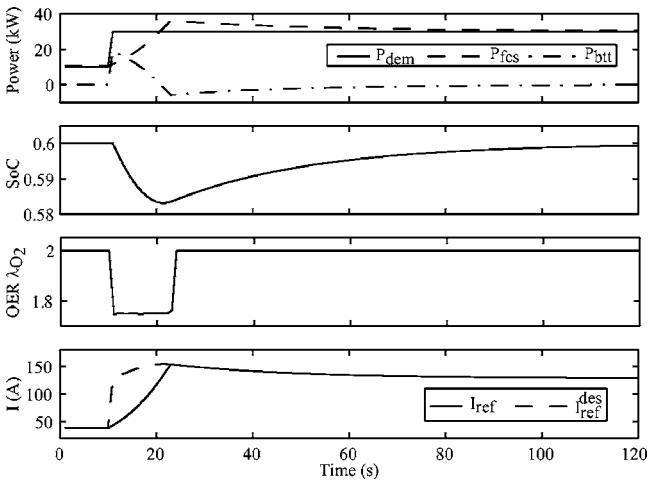

Fig. 8 Step response of the proportional controller with a time constant τ=30 s, an OER limit $\lambda_{O_2}^{lim}$=1.75, and a vehicle with a battery pack with ten modules. The power demand P_{dem} with a step from 10 kW to 30 kw (top, solid) and the FCS output power (top, dashed). The resulting SoC and OER (middle two) and reference current (bottom).

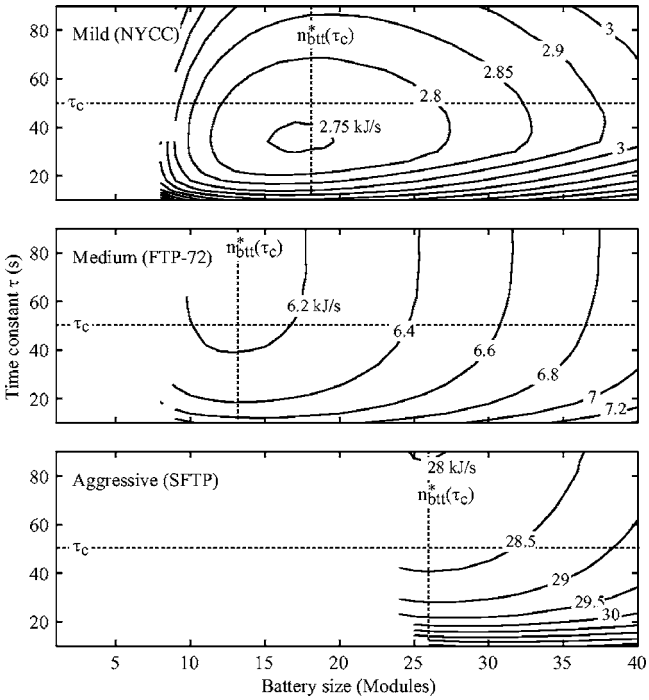

Fig. 9 Average energy loss for the proportional controller for the three drive cycles, with different battery sizes and time constants τ. The OER limit, $\lambda_{O_2}^{lim}$, is set to 1.75.

troller. The approach used is a linear proportional controller (PC) controlling an exact linearization of the process. The resulting system then becomes a first-order system with a time constant τ given by the PC. An overview of the proposed controller is shown in Fig. 1(*b*).

4.1 Proportional Controller With Exact Linearization. The model can be exactly linearized and controlled by a linear controller. This is done by using the desired change in state of charge as input, the reference current as output, the power demand as a disturbance, and calculating an inverse version of the FCHEV model in the controller. Hence the overall system response, for the battery state of charge, will have the characteristics of a linear system. The battery state of charge is compared to the reference state of charge (SoC_{ref}=0.6 as discussed above) to form an error that the controller needs to compensate for. The error in the state of charge is then scaled to form the desired change in the state of charge

$$\Delta SoC^{des} = \frac{1}{\tau}[SoC_{ref} - SoC(k)] \tag{19}$$

A large value for the constant τ, for example, corresponds to slow rate of battery charging after an initial discharge. The desired battery current I_{btt}^{des} for a desired change in state of charge, ΔSoC^{des}, is

$$I_{btt}^{des}(\Delta SoC^{des}) = \frac{-3600 q_{btt} \Delta SoC^{des}}{\eta_{btt}(\Delta SoC^{des})} \text{ [A]} \tag{20}$$

where the battery charging efficiency η_{btt} is

$$\eta_{btt}(\Delta SoC^{des}) = \begin{cases} 1 & \Delta SoC^{des} < 0 \\ 0.9 & \Delta SoC^{des} > 0 \end{cases} \tag{21}$$

The desired battery output power P_{btt}^{des} is then

$$P_{btt}^{des}(\Delta SoC^{des}) = \frac{V_{oc}^2 - (V_{oc} - 2I_{btt}^{des}(\Delta SoC^{des})R_{int})^2}{4R_{int}} \text{ [W]} \tag{22}$$

and the desired FCS output power

$$P_{FCS}^{des}(\Delta SoC^{des}) = P_{acc} - P_{btt}^{des}(\Delta SoC^{des}) + P_{aux} \text{ [W]} \tag{23}$$

where the power demand, P_{acc}, is known to the controller. The FCS power output map [1], denoted $P_{fcs}=f(I_{ref})$, is a monotonically increasing function for $I_{ref} < I_{ref}^{max}$=248 A and hence has the inverse $I_{ref}=f^{-1}(P_{fcs})$. The exact linearization of the model from the change in SoC, ΔSoC, to the reference current I_{ref} is then

$$I_{ref}^{des}(\Delta SoC^{des}) = f^{-1}[P_{fcs}^{des}(\Delta SoC^{des})] \text{ [A]} \tag{24}$$

The map in Fig. 2 used to calculate the OER

$$\lambda_{O_2}(k) = g[I_{ref}(k), I_{ref}(k) - I_{ref}(k-1)] \tag{25}$$

is monotonically decreasing with increasing $I_{ref}(k)$ for a given $I_{ref}(k-1)$. Hence, the function g has the partial inverse

$$I_{ref}^{max}\big|_{\lambda_{O_2}}(k) = g^{-1}[I_{ref}(k-1), \lambda_{O_2}^{lim}(k)] \text{ [A]} \tag{26}$$

where $I_{ref}^{max}|_{\lambda_{O_2}}$ is the maximum reference current that keeps the OER higher than $\lambda_{O_2}^{lim}$ for a given $I_{ref}(k-1)$. The desired reference current, I_{ref}^{des}, in the controller is limited by $\lambda_{O_2}^{lim}$

$$I_{ref}(k) = \min\left\{I_{ref}^{max}, I_{ref}^{max}\big|_{\lambda_{O_2}}(k), I_{ref}^{des}(k)\right\} \text{ [A]} \tag{27}$$

If $I_{ref}(k)=I_{ref}^{des}(k)$, i.e., the desired change in the SOC is slow enough that it does not require large FC currents, then the desired change in the battery SOC can be met and the actual battery charge since (19) becomes the closed-loop response,

$$SoC(k+1) - SoC(k) = \frac{1}{\tau}[SoC_{ref} - SoC(k)] \tag{28}$$

An example of a step in power demand and the resulting FCS power output, SoC, OER, I_{ref}^{des}, and I_{ref} are shown in Fig. 8. The example shows a vehicle with ten battery modules, a time constant τ=30 s, an OER limit of 1.75, and an initial power demand of 10 kW. The step of 20 kW shows that the desired reference current from the controller is limited by $\lambda_{O_2}^{lim}$ but that the SoC is finally regulated to the reference SoC, SoC_{ref}=0.6.

To compare the proportional controller to the DP optimizations the time constant τ must be investigated and set to a reasonably good value. Figure 9 shows the hydrogen equivalent total energy

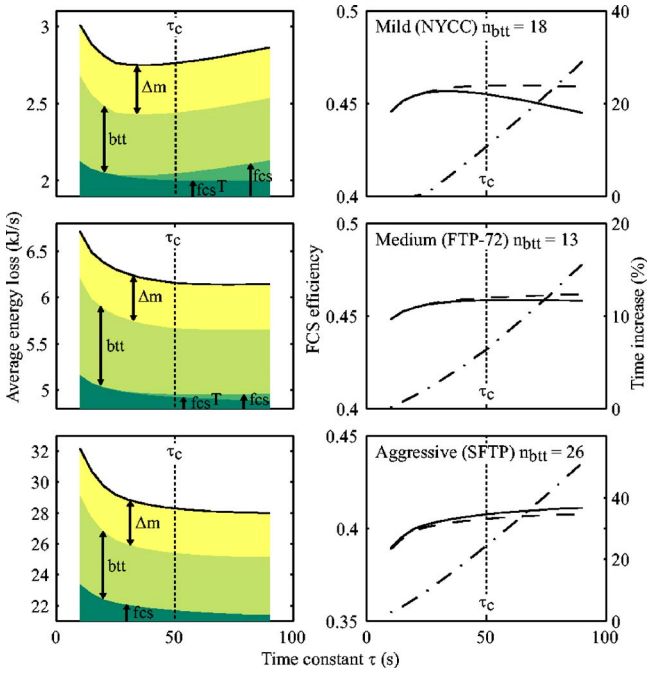

Fig. 10 The average energy loss per second (left column) in the three drive cycles when the proportional controller with different time constants controls the SoC (fixed battery size). Equivalent hydrogen energy loss from added weight (Δm), expended energy in the battery (btt), and total FCS energy loss (fcs), which comprises of the FCS energy loss during the cycle duration (fcs^T). Average FCS efficiency (right column) during the cycle duration (dashed) and total average FCS efficiency (solid) together with extra time used after the cycle duration (dashed dotted).

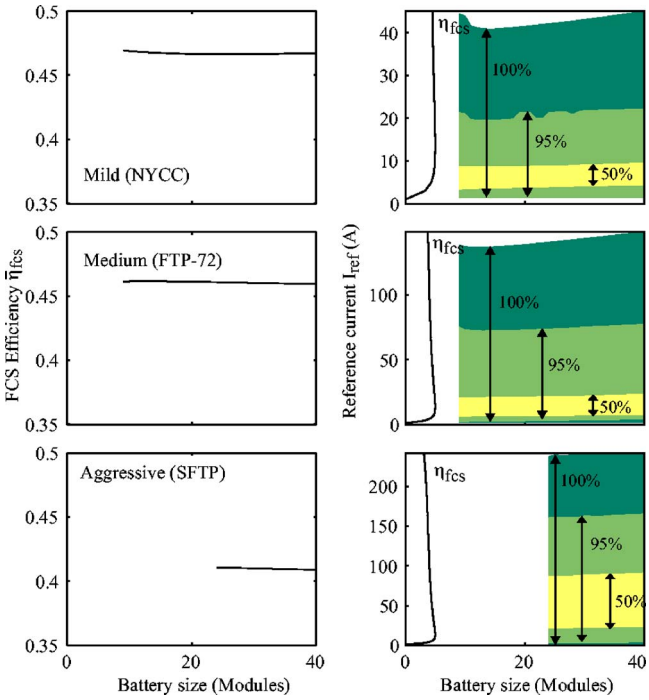

Fig. 11 Average FCS efficiency, $\bar{\eta}_{fcs}$, (left) together with the reference current distribution (right) for different battery sizes and drive cycles (when the PC, with τ_c=50 s, is controlling the SoC). The FCS efficiency curve is shown in the left part of the reference current distribution plot.

loss[4] of the vehicle with the PC controlling the SoC with an OER limit[5] of $\lambda_{O_2}^{lim}=1.75$, for the three drive cycles, with different time constants and battery sizes. The time constant has been varied between 10 s and 90 s.

The optimal pair of time constant and battery size, in Fig. 9, for each of the three drive cycles differ. A time constants τ_c=50 s is used to compare the proportional controller to the DP optimizations. Figure 9 shows both the time constant τ_c (horizontal dotted) and the corresponding optimal battery size $n_{btt}^*(\tau_c)$ (vertical dotted) for each of the cycles.

The longer time constant the more time is required, after the drive cycle's duration (Table 2), to recharge the battery to the reference state of charge SoC_{ref}. The right column of Fig. 10 shows the increase in total time (dashed dotted) when using different time constants. For example, using the time constant τ_c =50 s, the total time increases 24% from the original cycle duration (Table 2) for the aggressive cycle and 7% for the medium cycle.

In fact, the right column of Fig. 10 shows the average FCS efficiency during the original cycle duration (dashed) and the total average FCS efficiency, including the extra time used to recharge the battery (solid). For the mild cycle, the FCS operation after the cycle duration decreases the average FCS efficiency. Though, for the aggressive cycle the FCS operation after the cycle duration increases the average FCS efficiency. This explains why the total energy loss increases when increasing the time constant for the mild cycle and that an increase in time constant for the aggressive cycles lowers the overall energy loss.

Furthermore, the total hydrogen energy loss (separated into energy loss due to added mass (Δm), energy expended in the battery (btt), energy loss in the FCS during the cycle's duration (fcs^T) and the total energy loss in the FCS (fcs)) for different time constants, using, respectively, the cycle's optimal battery sizes $n_{btt}^*(\tau_c)$ (Fig. 9), is shown in the left column of Fig. 10. Note that the left column of Fig. 10 corresponds to the lines $n_{btt}^*(\tau_c)$ in Fig. 9. The energy loss due to the added mass (Δm) is now constant because of the fixed battery sizes. Figure 10 shows that the expended energy in the battery decreases slightly when increasing the time constant for all three cycles. The FCS energy loss at first decreases when increasing the time constant for all three cycles. However, the FCS energy loss increases for large time constants for the mild cycle and decreases for large time constants due to the different FCS efficiencies during the cycle and the period of recharging after the cycle.

4.2 Comparison to Dynamic Programming Optimizations. The effects of the battery size to the system efficiency when using the PC instead of DP differs in two fundamental ways. First, as shown in Fig. 11 (left column), the FCS efficiency does not increase when increasing the battery size. The reference current distribution (right column) is relatively the same for the different battery sizes. The constant FCS efficiency and reference current distribution is caused by the fact that the PC is designed to use the FCS as much as possible, without violating the OER constraints, and will therefore not, as the DP, exploit the opportunity of using the battery to increase the FCS efficiency.

Second, the minimal battery size with which the controller (i) was able to control the SoC and (ii) maintain an OER higher than the limit $\lambda_{O_2}^{lim}$ without exceeding the maximum output power of the

[4]Note that the PC does *not* ensure that $SoC(T)\approx SoC(0)$. The PC is therefore allowed to recharge the battery after the end of the cycle. However, the average energy losses, which includes losses after the cycle, are calculated per second of the cycle length (in Table 2).

[5]Note that if the OER limit, $\lambda_{O_2}^{lim}$, is set to zero, thus disregarding the OER dynamics, the controller would, for the mild and medium cycle, only use the FCS as power source making the battery useless.

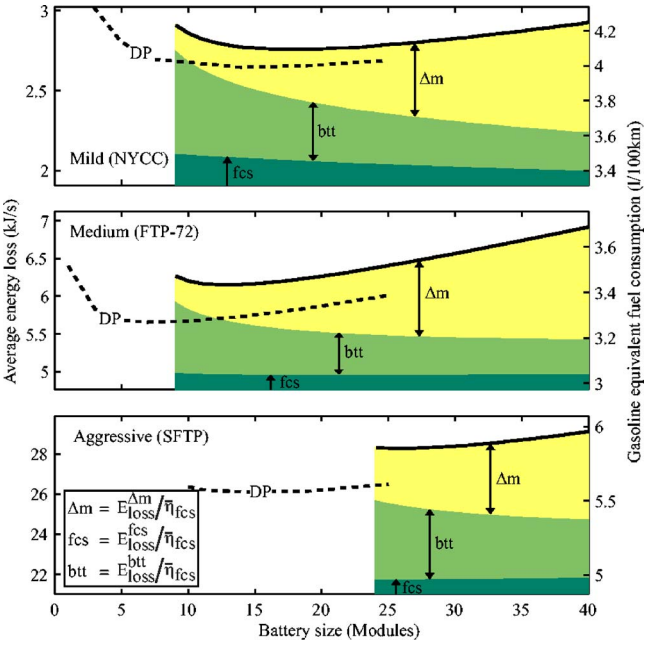

Fig. 12 The average energy loss per second in the three drive cycles when the proportional controller, with τ_c=50 s, controls the SoC. Equivalent hydrogen energy loss from added weight $E^{\Delta m}_{loss}/\bar{\eta}_{fcs}$ (Δm), expended energy in the battery $E^{btt}_{loss}/\bar{\eta}_{fcs}$ (btt), and FCS energy loss $E^{fcs}_{loss}/\bar{\eta}_{fcs}$ (fcs). The solid line shows the gasoline equivalent fuel consumption C^V_{gas}.

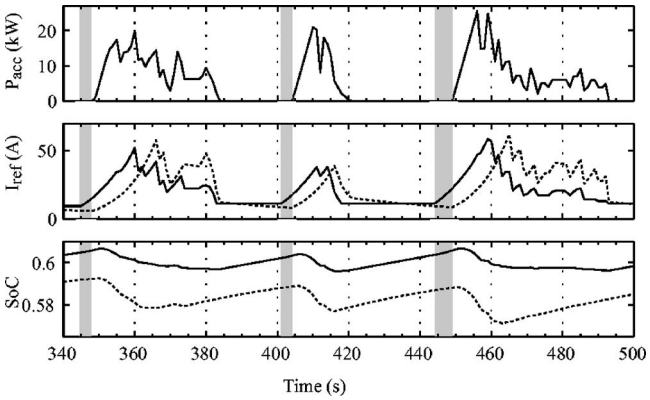

Fig. 13 Acceleration power demand (top) for a vehicle with ten battery modules for a portion of the medium FTP-72 cycle. The reference current (middle) and the battery state of charge (bottom) for both the DP (solid) and the PC with τ_c=50 s (dotted).

battery, is larger than the one specified by the DP (see Sec. 3.2). Both for the mild NYCC cycle and the medium FTP-72 cycle the minimum battery size when using the proportional controller is nine modules. For the aggressive SFTP cycle, the minimum battery size is 24 modules. The DP, however, managed to control the SoC for a battery pack with three modules, due to OER values below $\lambda^{lim}_{O_2}$ for a smaller battery sizes (Fig. 5) for both the mild and the medium cycle. For the aggressive cycle, using DP, the minimum size is 13 modules for the same reason.

Figure 12 shows the average energy losses, like in Sec. 3.2, separated in losses due to added mass, energy expended in the battery, and remaining losses in the FCS when the proportional controller controls the SoC. Note that Fig. 12 corresponds to τ_c =50 s in Fig. 9. The expended energy in the battery (btt), which, as in Sec. 3.2, decreases with increasing battery size because large battery sizes are more efficient than small when handling the same amount of power. The energy loss due to the added mass (Δm) is similar as in Sec. 3.2 because the corresponding electric energy loss does not depend on the controller type.

Even though the minimum sizes are larger than those using DP, there are optimal sizes for all three cycles. For the mild cycle, the optimal battery size is 18 modules, 13 modules for the medium cycle, and 26 modules for the aggressive cycle. These optimal sizes are caused, as in Sec. 3.2, by the large energy expended in the battery for relative small battery sizes and by the increasing energy loss due to the added weight for larger sizes.

The larger optimal sizes, when using the proportional controller, are due to the fact that the simple controller does not have any knowledge of the future at all. Hence, the controller can not maintain the reference current on a high level to prepare for future large increases in power demand. Figure 13 shows a time plot of the acceleration power demand, reference current, and state of charge when DP (solid), and the PC (dotted) are controlling the state of charge during a portion the medium cycle. The reference current profiles shows that DP reacts earlier (gray areas), even though the OER is limited, than the PC for increasing power demands. In fact, the DP increases the FCS reference current before the acceleration power demand increases due to the predictive nature of the DP strategy. This explains why DP is able to utilize smaller batteries than the PC, thus the different minimum battery sizes.

One improvement of the PC could be to not only limit the positive FCS reference currents changes but also including a similar OER map, Fig. 2, for negative transients. This could prepare the PC for increases in the FCS reference current and produce a more load-leveling profile.

Because the proposed controller is very simple and the DP is an optimal controller, a suggestion of a range of battery sizes can be made for each cycle. For the mild cycle, the optimal battery size range from 15 to 18 modules, for the medium cycle 7–13 modules, and for the aggressive cycle 15–26 modules.

Note that for the mild cycle, the optimal sizes only differ three modules while the difference for the medium cycle is six modules and 11 modules in the aggressive cycle. This is an indication of that, for the mild cycle, the optimal battery size is somewhat independent of the controller while there is, for the medium and definitely for the aggressive cycles an opportunity for battery downsizing when optimizing the controller.

5 Conclusions and Future Work

This paper shows that, for the considered vehicle, hybridization could be beneficial in terms of reduced hydrogen consumption when excursions in OER from a nominal value is penalized. First, the dynamic programming approach suggests an optimal battery size for every drive cycle. Second, the battery sizing when using the proposed nonlinear causal controller shows that the optimal battery sizes is larger than when using DP. However, the optimal battery size differs less for the mild cycle than for the medium and the aggressive cycles, indicating that the hybridization needs for the mild cycle could be independent of the control strategy.

The optimal battery size depends on the cycle, the vehicle weight, the type of battery, and energy density of the battery. Thus, this study is very specific to our configuration, the specific weights, and characteristics of the vehicle and its different components. Furthermore, the cost function when using DP influences, in general, the optimal results and, in particular, the optimal battery sizes in this study. The model used in this study is very simple and does not consider mechanical losses in the power train. The results can however be seen as an indication of how the optimal battery size change when considering the FCS transient loading compared to when disregarding the OER [1].

A stochastic dynamic programming approach will provide a causal stochastic optimal control law, for a given stochastic drive-cycle model, which could provide an interesting comparison to the

deterministic DP and the fixed structure controller results. In future work, this study could be performed under fixed vehicle net power by resizing battery and FCS, simultaneously. Resizing the FCS depend on scalable FCS auxiliary losses and associated transient response.

Acknowledgment

This work is supported by the National Science Foundation Grant No. CMS-0201332 and the Automotive Research Center with partial funding from Ford Motor Company.

Appendix: Dynamic Programming Algorithm

To optimally control

$$x_{k+1} = f(x_k, u_k, w_k) + x_k \tag{A1}$$

with the state x_k=SoC, the reference current as the input $u_k = I_{\text{ref}}$, and the power demand as the disturbance $w_k = P_{\text{dem}}$. The variables x_k, u_k, and w_k are limited to the finite spaces X, U, and W with $x_k \in X$, $u_k \in U$, $w_k \in W$. The DP algorithm allows us to find the control sequence $u=(u_o, \ldots, u_{k-1})$ that minimizes the cost function

$$\sum_{\tau=0}^{\tau=K} J(x_\tau, u_\tau) \rightarrow \min \tag{A2}$$

where $J(x_\tau, u_\tau)$ is the cost to use the input u_τ at the state x_τ. The cost J is defined as $J=(\alpha \Delta\text{SoC})^2 + \beta W_{\text{H}_2}$, where ΔSoC is the deviation of the battery's state of charge from the reference value SoC_{ref}, W_{H_2} is the hydrogen consumption in the FCS, and $\{\alpha, \beta\}$ are weights.

To solve the optimal control problem (A2), we need to define an intermediate problem that starts at time k with an initial state x_k. Let us define $V(x_k, k)$ the optimal cost to go or value function that will be incurred if the system starts at state x_k at time k and continues to the final time K,

$$V(x_k, k) = \min_{u(k), u(k+1), \ldots, u(K-1)} \sum_{\tau=k}^{\tau=K-1} J(x_\tau, u_\tau, w_\tau) \tag{A3}$$

with the final penalty $V(x_K, K) = (\delta \Delta\text{SoC})^2$, $\delta = 10^3$. The final state x_K at time K is penalized to ensure that the final state of charge is close to the initial state of charge. We then obtain a relationship that relates the value function at a certain point in time to the value function at a later point in time. Let x_m be the state at time m, and suppose that $(u_m, u_{m+1}, \ldots, u_{K-1})$ is a given control sequence that generates the trajectory $x_m, x_{m+1}, \ldots, x_K$. Let l be the anytime instance that satisfies $m < l \leq K-1$. The value function satisfies

$$V(x_m, m) = \sum_{\tau=m}^{\tau=l-1} J(x_\tau^*, u_\tau^*) + V(x_l^*, l) = \min_{u(m), \ldots, u(l-1)} \times \left[\sum_{\tau=m}^{\tau=l-1} J(x_\tau, u_\tau) + V(x_l, l) \right] \tag{A4}$$

which is the principle of optimality. In other words if $u_m^*, \ldots, u_l^*, \ldots, u_{K-1}^*$ is optimal for the problem starting at $k=m$ and $x_m^*, \ldots, x_l^*, \ldots, x_K^*$ is the resulting trajectory, then $u_l^*, \ldots, u_{K-1}^*$ is optimal for the problem that starts at $k=l$ with initial condition x_l^*. Finally, consider $m=k-1$ and $l=k$ then the Bellman equation [2] is obtained

$$V(x_{k-1}, k-1) = \min_{u_{k-1}} [J(x_{k-1}, u_{k-1}) + V(x_k, k)] \tag{A5}$$

which allows the calculation of the optimal control sequence backward starting from $k=K$. For more technicalities on the algorithm and the grid see [11].

References

[1] Sundstroem, O., and Stefanopoulou, A. 2007, "Optimum Battery Size for Fuel Cell Hybrid Electric Vehicle—Part 1," ASME J. Fuel Cell Sci. Technol., **4**(2), pp. 167–175.

[2] Bellman, R. E., 1957, *Dynamic Programming*, Princeton University Press, Princeton.

[3] Friedman, D. J., 1999, "Maximizing Direct-Hydrogen Pem Fuel Cell Vehicle Efficiency—Is Hybridization Necessary," SAE Paper No. SP-1425.

[4] Matsumoto, T., Watanabe, N., Sugiura, H., and Ishikawa, T., 2002, "Development of Fuel-Cell Hybrid Vehicle," SAE Paper No. 2002-01-0096 SP-1691.

[5] Lin, C. C., Peng, H., and Grizzle, J. W., 2004, "A Stochastic Control Strategy for Hybrid Electric Vehicles," *Proc. of American Control Conference*, Boston, AACC & IEEE, New York, pp. 4710–4715.

[6] Ishikawa, T., Hamaguchi, S., Shimizu, T., Yano, T., Sasaki, S., Kato, K., Ando, M., and Yoshida, H., 2004, "Development of Next Generation Fuel-Cell Hybrid System—Consideration of High Voltage System," SAE Paper NO. 2004-01-1304. SP-1827.

[7] Jeong, K. S., and Oh, B. S., 2002, "Fuel Economy and, Life-Cycle Cost Analysis of a Fuel Cell Hybrid Vehicle," J. Power Sources, **105**, pp. 58–65.

[8] Suh, K.-W., and Stefanopoulou, A. G., 2006, "Effects of Control Strategy and Calibration on Hybridization Level and Fuel Economy in Fuel Cell Hybrid Electric Vehicle," SAE Paper No. 2006-01-0038.

[9] Pukrushpan, J. T., Stefanopoulou, A. G., and Peng, H., 2004, "Control of Fuel Cell Breathing," IEEE Control Syst. Mag., **24**(2), pp. 30–46.

[10] Johnson, V. H., 2002, "Battery Performance Models in Advisor," J. Power Sources, **110**, pp. 321–329.

[11] Sundstroem, O., 2006, "Optimal Power Split in Fuel Cell Hybrid Electric Vehicle With Different Battery Sizes, Drive Cycles, and Objectives," Master's thesis, Chalmers University of Technology, Gothenburg, Sweden.